X-671-70-367
PREPRINT

THE HeI LINE PROFILES IN NORMAL B TYPE SPECTRA

DAVID S. LECKRONE

SEPTEMBER 1970

GODDARD SPACE FLIGHT CENTER
GREENBELT, MARYLAND

THE HeI LINE PROFILES IN NORMAL B TYPE SPECTRA

David S. Leckrone
National Aeronautics and Space Administration
Goddard Space Flight Center
Greenbelt, Maryland

September, 1970

Submitted for Publication
to Astronomy and Astrophysics

SUMMARY

The primary aim of this study is to determine to what extent the profiles of a large number of HeI lines, as observed over the entire range of B spectral types, can be matched by theoretical profiles computed in LTE. Detailed profile analyses of as many as 11 HeI lines, carried out for the stars 134 Tau (B9 IV), π Cet (B7 V), HR 2154 (B5 IV), ϵ Her (B3 V), γ Peg (B2 V), HR 1861 (B1 V) and υ Ori (B0 V), are summarized. Original, high dispersion profile data are presented for five of these stars.

Stellar log g and T_{eff} values are estimated from Hγ and Hδ profiles and spectrophotometric data, reduced to the new standard calibration of Vega by Oke and Schild (1970). The observed MgII λ4481 profiles yield V sin i values <30 km/sec for all the stars considered and yield an average log N(Mg)/N(H) + 12 = 7.8 $\pm$ 0.1.

For most of the HeI lines considered at spectral types B1 and B0, one cannot match simultaneously an observed line core and the observed line wings with an LTE profile; the observed cores are systematically deeper and broader than predicted. For certain lines ($\lambda\lambda$4471, 5876, 6678 and possibly $\lambda\lambda$4026, 4388) this problem persists over the entire range of spectral types considered (B0-B9). The observed singlet/triplet equivalent width ratios are well reproduced by the LTE calculations in spite of evident deviations from LTE in the line cores.

Estimated He/H ratios, obtained on the basis of theoretical fits to the weaker HeI lines and to the wings of the strong lines, are given for six of the seven stars considered. An overall average N(He)/N(H) = 0.106 is obtained for these stars, from a total of 46 lines, with little scatter being noted in the results obtained from line to line for a given star. Virtually no scatter exists in the derived He/H ratios among the six stars considered. It is unlikely that the more obvious sources of possible systematic errors could push the average N(He)/N(H) for these stars outside the range 0.095-0.125. Derived He/H ratios for υ Ori and HR 1861, members of the Orion association, are in excellent agreement with the results of recent optical studies of the Orion nebula. The need for a rigorous theoretical test of the LTE assumption for the weak HeI lines and the wings of the strong lines is stressed.

Key words: B stars - helium abundances - line profiles - non LTE.

I. INTRODUCTION

The determination of the He/H abundance ratio for nearby main-sequence stars and diffuse nebulae and the detection of possible variations in its value as a function of position in the galaxy or population membership has bearing on a variety of astrophysical problems. Principal among these is the development of a coherent picture of the history of stellar nucleosynthesis and chemical enrichment of the interstellar medium. Ultimately, such a model may be used to infer the helium content of the primeval material from which the galaxy formed, a datum pertinent to the development of cosmological models. A general review of these problems has been given by Tayler (1967).

Insofar as objects of solar age or younger are concerned, the He/H ratio may be estimated by means of at least five methods: solar flare cosmic ray observations, stellar mass-luminosity relation studies, observations of HII region recombination lines at optical wavelengths, observations of HII region radio recombination lines, and studies of the helium absorption line spectra of early type stars. The credibility of results obtained by any of these methods rests upon the verification of the physical assumptions made in each type of study and the demonstration that He/H ratios obtained for the same or similar objects by different methods are consistent.

The present work deals specifically with the interpretation of the profiles of HeI absorption lines observed in normal, main-sequence B star spectra. Early studies along similar lines were hampered by the lack of an adequate Stark broadening theory for the HeI lines and by the inadequacies of available model atmospheres (Underhill, 1953, 1966; Aller and Jugaku, 1959). Helium abundances derived in such studies typically lay in the range $0.12 \lesssim N(He)/N(H) \lesssim 0.20$, by number of atoms (Traving, 1955, 1957; Jugaku, 1957, 1959; Aller and Jugaku, 1959; Mihalas, 1964). On the other hand, He/H ratios derived in studies of spiral arm diffuse nebulae, in studies of the mass-luminosity relation for binary stars and in solar studies have consistently yielded He/H ratios $\lesssim 0.12$ (Tayler, 1967; Durgaprasad et al., 1968; Peimbert and Costero, 1969; Peimbert and Spinrad, 1970; Popper et al., 1970; Bahcall and Ulrich, 1970). The weight of evidence from nebular, binary star and solar work, coupled with the theoretical difficulties involved in model atmospheres analyses tended to raise serious doubts about the reliability of the stellar spectroscopic results.

Quantum mechanical calculations of Stark profile functions are now available for most of the HeI lines of interest, as are large grids of B star model atmospheres. Consequently, a number of workers have recently readdressed the problem of interpreting stellar HeI spectra. These studies may be

divided into two groups - those which utilized equivalent width data alone and those which attempted to match theoretically the observed HeI line profiles.

Equivalent width data for the weak HeI line, λ4713, as observed at spectral types B5 and earlier, were used by Hyland (1967) in estimating the helium content of two southern galactic clusters. Shipman and Strom (1970) utilized published equivalent widths for a single strong HeI line, λ4471, in estimating the He/H ratio for a large number of B stars. Both Hyland and Shipman and Strom obtained values of N(He)/N(H) $\approx$ 0.09-0.10, although substantially higher values were derived for a few stars. Baschek and Norris (1970) have carried out equivalent width analyses of many HeI lines for γ Pegasi, a B2 V star. They estimate N(He)/N(H) = 0.11.

Detailed analyses of HeI line profiles have recently appeared in conjunction with the study of five B stars: the two B0 stars τ Scorpi and λ Leporis (Hardorp and Scholz, 1970) and three B3 stars, ι Herculis, η Hydrae and HD 58343 (Kodaira and Scholz, 1970). Hardorp and Scholz estimate values of N(He)/N(H) $\approx$ 0.10, while Kodaira and Scholz obtain a much lower average, $\approx$ 0.06. The very low He/H ratios derived by Kodaira and Scholz appear to be the consequence of a choice of stellar effective temperatures significantly hotter than one would expect for B3 stars (see Section IV).

All of these studies are based upon the fundamental physical assumption that the HeI lines are formed under

local thermodynamic equilibrium (LTE). Each is limited either in the range of spectral types covered or in the number of HeI lines considered. No detailed modern analysis of the HeI line profiles of stars of spectral type later than B3 has appeared prior to the present study, for example.

The exclusive use of equivalent width data in estimating abundances from strong spectral lines, including those of HeI, is a hazardous procedure. Not only may important physical effects be overlooked in such an approach, but poor matches between theory and observations may be camouflaged in a systematic way. The profile analyses of Hardorp and Scholz indicated that only the weakest HeI line profiles could be completely matched at spectral type B0. The observed cores of the stronger lines were invariably deeper than predicted. Snijders and Underhill (1970) have shown qualitatively that the observed core of HeI λ4471 is markedly deeper than the published theoretical profiles of Shipman and Strom would indicate, at least at spectral types B5 and earlier. The calculations of Johnson and Poland (1969) and of Poland (1970) indicate that the cores of some HeI lines may indeed be deepened by non-LTE effects; while little difference between LTE and non-LTE profiles is found in the line wings. However, the adequacy of Johnson and Poland's non-LTE calculations has been questioned by Snijders and Underhill, who suggest that non-LTE effects may be important even at the great atmospheric depths where the weak HeI lines and the wings of the strong lines are formed. Hummer and

Mihalas (1967) have pointed out that non-coherent scattering by free electrons may also serve to deepen and broaden the cores of strong lines.

The primary aim of the present study is to determine to what extent the profiles of a large number of HeI lines, both weak and strong, both isolated and hydrogenic, as observed over the entire range of B spectral types, can be matched by theoretical profiles computed in LTE. It is hoped that this will provide a framework of empirical data on the basis of which the scope of the non-LTE problem may be defined. In those cases where the entire observed profile of a weak line or the wings of a stronger HeI line are well matched by the LTE calculations, an estimate of the He/H ratio may be obtained.

Detailed profile analyses of as many as eleven HeI lines have been carried out for each of seven stars, ranging in spectral type from B9 to B0. Original, high dispersion profile data are presented for five of these stars. Helium abundance estimates are obtained from a sufficient number of lines in each case so that a reasonable estimate of the random errors involved in the analyses may be made. The physical significance of the abundances so derived must ultimately depend upon the future demonstration that the LTE assumption is indeed valid for those deep atmospheric regions where the weak HeI lines and the wings of the stronger lines are formed.

II. THE OBSERVATIONS

The stars chosen for this investigation are bright, virtually unreddened and sharp-lined objects. Table 1 lists spectral type and photometric data for each, as taken from the Bright Star Catalogue (Hoffleit, 1964) and from the compilation of Johnson et al. (1966). Also given is the approximate projected rotational velocity, V sin i, for each star, obtained from low dispersion spectra by Slettebak (1954) and Slettebak and Howard (1955). The rotational velocities derived in section V, on the basis of high resolution data, for five of the stars differ from those given in Table 1 by as much as 18 km/sec in some cases. In each instance, V sin i lies below 30 km/sec, however.

Two types of observations were required for this study: high dispersion photographic spectra and photoelectric scans of the stellar continuous energy distributions or alternative photometric data. The photographic spectra provided profile data for the HeI lines, the hydrogen Balmer lines and the MgII λ4481 line. The use of the Hγ and Hδ profiles together with the continuous energy distributions or other photometric data in fitting model atmospheres to the program stars is discussed in section IV. Section V describes the estimation of the stellar V sin i values, by use of the MgII λ4481 profile. The paragraphs below outline primarily the observations and reductions original to this paper.

High dispersion spectra of 134 Tauri, π Ceti, HR 2154, HR 1861 and υ Orionis were obtained by the author, under the guidance of Professor L.H. Aller, with the coude spectrograph of the 120-inch telescope at the Lick Observatory during October, 1967. The observing program incorporated three distinct instrumental combinations, the characteristics of which are summarized in Table 2. Column 8 of Table 1 indicate the systems utilized for each star observed.

Two of the stars, HR 2154 and HR 1861, are binaries with faint companions. Light from the companion of HR 2154 was not allowed to enter the spectrograph slit. The companion of HR 1861 was not observed, but it is sufficiently faint relative to the program star ($\Delta m_V = 4.5$) as to be of only minor concern here. Subsequent examination of the plate tracings of HR 1861 revealed no apparent evidence of spectral contamination by the fainter star.

A Grant Mark III microphotometer, utilized in the density mode, provided tracings of each of the photographic spectra. Great care was exercised in tracing each of the line profiles of interest. The fog level, plate calibration data and spectrum profile (perpendicular to the dispersion) appropriate to each line were determined at points on the plate as close to the line as possible. Tracings of nearby comparison lines yielded an estimate of the tracing scale in Å/inch for each line. The results were found to be reproducible

from plate to plate for a given line to within one part in five hundred.

Comparison line profiles yielded estimates of the instrumental broadening functions for each of the three systems summarized in Table 2. The sharp lines emitted by the comparison spectrum source, an iron-neon hollow cathode tube, are well suited for this purpose. The estimates of the instrumental resolution listed in Table 2 correspond simply to the half-intensity widths of the normalized instrumental profiles so obtained. Instrumental broadening proved to be of significance only in the case of the 8Å/mm data.

All profile data (both "signal" and "noise") were processed with an analogue-to-digital converter and were then reduced from density to intensity units by means of a computer code developed by Ross (Aller and Ross, 1967). This code incorporates a correction to the plate calibration curves for the effects of non-uniform spectrum widening.

For the purposes of this investigation it was necessary to idealize the profile data in the sense that a smoothed mean was fitted through the random noise in each case. Thus, the profiles tabulated or illustrated in subsequent sections necessarily reflect the subjective judgement of the author. The corresponding intensity profiles in their original signal-plus-noise form may be found in the author's thesis (Leckrone, 1969).

Multiple observations of only a few profiles were obtained. Different observations of the same line agreed with each other for the most part to within one per cent of the continuum (residual flux units), although larger uncertainties ($\sim \pm 3\%$) may be expected near the centers of the deepest line profiles observed (with residual fluxes $\lesssim 0.50$). A second test of the quality of the data, the consistency of He/H ratios derived from different lines observed for the same star, will be discussed in section VI.

HeI, HI and MgII λ4481 profile and equivalent width data for γ Peg and ι Her have also been utilized in this study. The γ Peg data were taken from Aller (1956), Jugaku (1957) and Aller and Jugaku (1959). The HeI equivalent width data for ι Her are those given by Peters and Aller (1970), while a limited amount of HeI profile data for ι Her has been provided to the author by Mrs. Peters. Instrumental broadening functions were not available for use with the γ Peg or ι Her data.

Continuous energy distributions for π Ceti, ι Her, γ Peg and υ Ori are available in the literature (Wolff et al., 1968; Jugaku and Sargent, 1968; Code, 1960). The author obtained photoelectric spectrum scans for 134 Tauri, HR 2154 and three standard stars (ε Ori, η Hya and γ Gem) with the Wampler scanner (Wampler, 1966), mounted at the prime focus of the 36-inch Crossley reflector at Lick Observatory in November, 1968. The instrumentation utilized was virtually

identical to that used by Wolff et al. (1968) and by Hayes (1970). The wavelength range $\lambda\lambda$3200-5263 was observed in 2nd order with a 49Å bandpass, while the range $\lambda\lambda$5263-7550 was observed in 1st order with a 33Å bandpass. The data were reduced according to the procedures outlined by Oke (1965) and by Hayes (1970), extinction data, paired pulse corrections, etc., being taken from the latter reference. The question of the calibration of the observed spectral energy distributions with reference to the primary standard, α Lyrae, is discussed in section IV.

No spectral energy distribution data for HR 1861 are currently available. Its effective temperature was estimated by use of the relation between the reddening-independent parameter, Q = (U-B) - 0.72(B-V), and T_{eff} predicted from the grid of model atmospheres utilized (see Section IV).

The line profile data and observed continuous energy distributions which are original to this paper are either tabulated or illustrated in later sections.

III. THEORETICAL LINE PROFILE CALCULATIONS

The theoretical (LTE) profiles of eleven HeI lines, Hγ, Hδ and the MgII λ4481 doublet were generated by straightforward Simpson's rule quadratures of the flux integrals

$$F_\lambda(\Delta\lambda) = 2\pi \int_{-\infty}^{+\infty} S_\lambda(x,\Delta\lambda)\, E_2\,[\tau_\lambda(x;\Delta\lambda)]\, \frac{[\kappa_\lambda(x) + \sigma_\lambda(x) + 1_\lambda(x,\Delta\lambda)]}{[\kappa_o(x) + \sigma_o(x)]}\, \frac{10^x}{M}\, dx \qquad (1)$$

and

$$F_\lambda^c = 2\pi \int_{-\infty}^{+\infty} S_\lambda^c(x)\, E_2\,[\tau_\lambda^c(x)]\, \frac{[\kappa_\lambda(x) + \sigma_\lambda(x)]}{[\kappa_o(x) + \sigma_o(x)]}\, \frac{10^x}{M}\, dx \qquad (2)$$

for the line plus continuum and the continuum alone, respectively. The flux integrations were carried out over model atmospheres available in the literature (section IV). In equations (1) and (2) λ denotes the central wavelength of the line. κ_λ, σ_λ and 1_λ are the continuous absorption coefficient, the scattering coefficient for the continuum and the line absorption coefficient, respectively. κ_o and σ_o denote absorption and scattering coefficients at a standard wavelength. $\tau_\lambda(x,\Delta\lambda)$ is the total optical depth in the line plus continuum, while $\tau_\lambda^c(x)$ denotes the optical depth in the

continuum alone. The variable x is a depth parameter defined by

$$x = \log \tau_c^d , \tag{3}$$

where τ_o^c is the continuum optical depth at the standard wavelength. $M = \log_{10} e$. Both observed and theoretical profiles discussed throughout this paper are in the normalized form

$$R_\lambda (\Delta\lambda) = \frac{F_\lambda (\Delta\lambda)}{F_\lambda^c} \tag{4}$$

These calculations took explicit account of scattering processes in the formation of the continuum so that, at a given atmospheric depth, the source function adopted for the combined line and continuum is given by

$$S_\lambda = \frac{(\varkappa_\lambda + \sigma_\lambda) S_\lambda^c + 1_\lambda B_\lambda}{\varkappa_\lambda + \sigma_\lambda + 1_\lambda} \tag{5}$$

while that for the continuum alone is

$$S_\lambda^c = \frac{\varkappa_\lambda B_\lambda + \sigma_\lambda \Lambda[S_\lambda^c]}{\varkappa_\lambda + \sigma_\lambda} \tag{6}$$

Here B_λ denotes the Planck function evaluated at the local electron temperature and $\Lambda[S_\lambda^c]$ represents the local value of the mean intensity in the continuum. S_λ^c was calculated iteratively, by use of the techniques outlined by Mihalas (1967a).

The sources of continuous opacity considered were bound-free and free-free transitions involving HI, HeI, HeII and H^-, absorption by H_2^+, coherent scattering by free electrons and Rayleigh scattering by atomic hydrogen. The opacity calculations followed those outlined by Mihalas (1967a) with the following exceptions: the HeI opacity was calculated in the manner described by Vardya (1964, corrected for typographical errors); the HI Gaunt factors were computed from polynomials given by Mihalas (1967b); and polynomials for the H^- free-free opacity were taken from Fischel (1963).

The line absorption coefficient is given in the usual notation (e.g. Aller, 1963) by

$$l_\lambda(x,\Delta\lambda) = n_{r,s}(x)\left[\frac{\pi e^2}{mc}\ f\right](1-e^{-hc/\lambda kT})\ \frac{\lambda^2}{c\Delta\lambda_D}\ \Phi_\lambda(x,\Delta\lambda). \qquad (7)$$

Here $n_{r,s}(x)$ is the number of atoms per gram of stellar material, in ionization state r and excitation state s, capable of absorbing radiation at a distance, $\Delta\lambda$, from the line center. It is the product of the Saha-Boltzmann factor, the number of hydrogen atoms per gram of stellar material and the abundance of the species in question relative to hydrogen, e.g. N(He)/N(H). In the calculation of $n_{r,s}(x)$ the partition

functions used for HeI and HI were those of de Jager and Neven (1960). The excitation and ionization potentials for HeI and HI were taken from Wiese, Smith and Glennon (1966), as were the f-values for the HeI lines. f-values for the Balmer lines were taken from Underhill and Waddell (1959), and the f-value used for MgII λ4481 is that given by Griem (1964). Table 3 summarizes the pertinent data for the HeI lines considered in this study. $\Delta\lambda_D$ in equation (7) is the line Doppler width, which accounts for both thermal and microturbulent processes. The calculations carried out here assume, for the most part, a zero microturbulent velocity, V_T. Evidence that prevailing V_T values must indeed be low for the stars in question is discussed in sections V and VI.

$\Phi_\lambda(x, \Delta\lambda)$ in equation (7) represents the absorption profile function per unit frequency interval for the line. Insofar as the HeI lines are concerned, it is easily shown that van der Waals broadening and resonance broadening are negligible when compared to Stark broadening, thermal Doppler broadening and radiation damping. For the hydrogen lines and the hydrogenic HeI lines only Stark broadening and thermal Doppler broadening need be taken into account.

The profile calculations for the isolated HeI lines utilized the Stark broadening parameters derived in the investigation of Griem et al. (1962). For these lines the ion broadening may be reasonably described in the phase-shift

limit of the impact approximation over the entire range of dwarf B star atmospheres, i.e. the parameter σ always falls below the lowest values tabulated by Griem et al., for the range of temperatures and electron densities of interest here. Under these circumstances, the Stark broadening function takes on the form of a dispersion profile. Thus, the combined Stark broadening, radiation damping and Doppler broadening for the isolated HeI lines were described by means of the well known Voigt function, H(a,v), with

$$a = \frac{w}{\Delta\lambda_D} \left[1 + 1.36\alpha^{8/9}\ \sigma^{-1/3}\right] + \frac{\Gamma_R}{4\pi\Delta\lambda_D} \qquad (8)$$

and

$$v = \frac{1}{\Delta\lambda_D} \left[\Delta\lambda - w\ \left(\frac{d}{w} \pm 2.36\ \alpha^{8/9}\sigma^{-1/3}\right)\right]. \qquad (9)$$

The parameters w, d/w, σ and α are tabulated by Griem et al. In equation (9) the minus sign applies to the blue-shifted lines ($\lambda\lambda$ 5016, 5876) while the plus sign holds for the red-shifted lines ($\lambda\lambda$ 4121, 4438, 4713, 5048, 6678). The radiation damping constants (Γ_R) for the isolated HeI lines were calculated by use of the Einstein coefficients given by Wiese et al. (1966). The appropriate values of H(a,v) were interpolated from the tables of Finn and Mugglestone (1965).

A similar approach was adopted for the MgII λ4481.13,.33 doublet. In this case the Stark broadening parameters were taken from Griem (1964) and the radiation damping was

calculated following Henry and Mihalas (1964). The MgII doublet was calculated as a blend of two resolved lines.

Quantum mechanical Stark broadening functions are available for a few of the hydrogenic HeI lines. The calculations of the λ4471 and λ4922 profiles employed Stark broadening functions tabulated by Barnard et al. (1969). The author is indebted to Dr. L. Shamey for providing similar profile functions for λ4026 and λ4388 in advance of publication. For $\lambda\lambda$4026, 4388, 4922 the far wings were assumed to vary as $\Delta\lambda^{-5/2}$. The variation with $\Delta\lambda$ of the far wings of λ4471 was taken to be that prescribed by Griem's (1968) equation 37. The extrapolated wings were convolved with the appropriate thermal Doppler profile in each case.

At electron densities lower than $10^{14}cm^{-3}$, Barnard et al. prescribe that the hydrogenic Stark profiles be approximated by dispersion profiles, with widths and shifts as given in their paper, and that the forbidden components of these lines be neglected at such low densities. This procedure was followed in the present calculations, except insofar as the Stark profile functions were forced to vary smoothly between their tabulated values at $N_e = 10^{14}cm^{-3}$ and their dispersion profile form at $N_e = 3 \times 10^{13}cm^{-3}$.

The semi-empirical formalism of Edmonds et al. (1967) was adopted in the calculation of the Balmer line Stark profiles.

The accuracy of the profile calculations was confirmed by a comparison with similar calculations carried out by Klinglesmith (1969, private communication; Hunger and Klinglesmith, 1969). Good agreement also obtains between the present calculations of the wings of the hydrogenic HeI lines and those calculated by Norris and Baschek (1970). It should be noted that the isolated HeI profiles calculated here seem to be slightly stronger than those computed under similar assumptions by Norris and Baschek.

Except for the analyses of ζ Her and γ Peg, each of the theoretical HeI profiles was folded with the appropriate instrumental and stellar rotational broadening functions before being compared to the observed profiles. The present treatment of rotational broadening follows the procedures summarized, for example, by Unsöld (1955, equation 123.12). The V sin i values used are those summarized in section V.

IV. THE CHOICE OF MODEL ATMOSPHERES

In the context of this study the terms "effective temperature" (T_{eff}) and "surface gravity" (log g) are applied to fitting parameters characteristic of a theoretical model atmosphere. The differences between these parameters and the corresponding physical quantities for a real star, with which the model has been associated, will depend upon the physical sophistication of the model, i.e. the extent to which line blanketing effects, deviations from LTE, convection, etc., have been accounted for. Unless otherwise noted, T_{eff} values in the range $16,800^{o}$ - $33,000^{o}$, mentioned in the following discussion, refer to the temperature scale defined by the line-blanketed models of Morton and his collaborators (Mihalas and Morton, 1965; Adams and Morton, 1968; Hickock and Morton, 1968; Bradley and Morton, 1969; Van Citters and Morton, 1970). Quoted T_{eff} values less then $16,800^{o}$ are those associated with the hydrogen line-blanketed models of Klinglesmith (1970). For the study of ι Her the Van Citters - Morton grid was supplemented with one unblanketed model ($T_{eff} = 20,200^{o}$, log g = 3.8) from the grid of Mihalas (1965). This was necessary for the proper definition of the maximum in the HeI line strength vs. T_{eff} relation. At log $\tau_{o} > -2.0$, where the weak HeI line and the wings of the strong lines are formed, the unblanketed Mihalas model should be nearly identical to a line-blanketed model with $T_{eff} = 18,700^{o}$.

No single grid of modern model atmospheres currently available in the literature is capable of describing the entire range of main-sequence B stars ($10{,}000^{\circ} \lesssim T_{eff} \lesssim 31{,}000^{\circ}$; $3.0 \lesssim \log g \lesssim 4.5$). The combination of grids referenced above covers the entire range of T_{eff} of interest and, at most effective temperatures, provides models for at least two log g values. It probably represents the best "patchwork" grid currently available. Its major deficiency is that is provides few models for values of log g > 4.0. Thus, for two of the stars investigated here (γ Peg and υ Ori) it was necessary to extrapolate computed quantities in order to estimate their values for log g slightly greater than 4.0.

The analysis of each star required a model atmosphere capable of reproducing simultaneously the observed Hγ and Hδ line profiles and the observed stellar continuous energy distribution - i.e. the slope of the Balmer continuum, the size of the Balmer discontinuity and the slope of the Paschen continuum. The primary determinant of T_{eff} for the B stars in question was, of course, the size of the Balmer discontinuity. Ambiguities in the observed slope of the Balmer continuum complicated the estimation of the size of this discontinuity in a few cases.

Two new calibrations of the continuous energy distribution of Vega, the primary spectrophotometric standard, have recently become available - that of Hayes (1970) and that of Oke and Schild (1970). These differ by about 0.05

mag. in the value obtained for Vega's Balmer discontinuity and also differ somewhat in the slope found for the Balmer continuum. The Balmer jump derived by Oke and Schild agrees with the earlier determination by Bahner (1963). Thus, effective temperatures determined from continuous energy distributions observed on the system defined by Hayes are cooler than those derived from observations referred to the system of Oke and Schild. The line profile analyses outlined in this paper are based upon T_{eff} values derived primarily from data reduced to the latter system. Results of similar analyses based upon effective temperatures determined relative to Hayes' calibration of α Lyrae, will be summarized in section VI.

The observed slope of the Balmer continuum for γ Peg (B2), when reduced to the Oke-Schild system, was noted to be substantially steeper than predicted by model atmospheres for effective temperatures in the range $20{,}000^{\circ}$-$22{,}000^{\circ}$. However, on the Hayes system observed and theoretical Balmer slopes could be well matched. The inverse problem was encountered for 134 Tauri (B9). On the Hayes system observed and theoretical Balmer slopes disagreed, while better agreement was obtained when the data were reduced to the Oke-Schild system. Such ambiguities, though puzzling, are of little consequence in this study. The T_{eff} derived for γ Peg on the Oke-Schild system may be as much as 600° too high because of the Balmer slope uncertainty, but γ Peg lies

near the maximum of the HeI line strength vs. T_{eff} relation. Thus, errors of several hundred degrees in T_{eff} have little effect on the HeI profiles or equivalent widths predicted for it.

The surface gravities derived here on the basis of the formalism of Edmonds et al. (1967), are higher by about 0.2 in log g than those one would derive by use of the Kolb-Griem theory (Strom and Peterson, 1968). The uncertainty in the He/H ratio derived for each star, due to systematic effects of this sort, will be discussed in section VI.

In no instance was it possible to match simultaneously the observed cores and the observed wings of the Balmer lines with the theoretical LTE profiles. In each case the observed cores of $H\gamma$ and $H\delta$ were significantly deeper than those predicted by the calculations. A particularly distressing example is that of the B0 star, υ Orionis, for which a good fit to the observed $H\delta$ profile could be obtained only for $\Delta\lambda \gtrsim 7\mathring{A}$. This is probably due to non-LTE effects, which influence only the Balmer line cores for $T_{eff} \lesssim 30{,}000^{o}$, but which begin to play an important role in the formation of the line wings as T_{eff} increases above $30{,}000^{o}$ (Mihalas and Auer, 1970; Auer, private communication, 1970).

Observational data which are original to the present study are summarized in tables 4 through 6. Table 4 contains the observed spectral energy distributions of 134 Tauri and HR 2154 reduced to the Oke-Schild system and normalized to $m_{\nu} = 0.00$

at λ = 5556Å. The Balmer line profiles are given in tables 5 and 6. Usable Hγ profiles were not obtained for 134 Tau, π Cet and υ Ori.

Table 7 compares T_{eff} and log g values obtained with continuous energy distributions observed relative to the Oke-Schild system to those obtained from the same data reduced to the Hayes system and, in a few cases, to those obtained by use of the Q vs. T_{eff} relation predicted by the model atmospheres. The T_{eff} derived from the observed Q value of HR 1861, for which no spectrum scan was available, should be correct to within about 1000°.

Kodaira and Scholz (1970) assumed an effective temperature of 18,700°, on the scale defined by blanketed model atmospheres, for ι Her (B3) in order to achieve ionization equilibria. This T_{eff} is 1200° - 1700° hotter than the value one derives from the observed Balmer discontinuity of ι Her, as determined by Shipman and Strom (1970), by Kodaira and Scholz themselves and by the author in the present study. The T_{eff} adopted by Kodaira and Scholz lies outside the range of uncertainty of the effective temperature derived from interferometric data by Hanbury Brown et al. (1967) for a star with this spectral type and color index ($\sim$ 17,000° $\pm$ 1300°). Moreover, it vastly exceeds the ionization balance temperature obtained by Peters and Aller (1970) for ι Her (17,000° for SII/SIII; 17,250° for SiII/SiIII). Kodaira and Scholz attribute the latter discordance to the failure of

Peters and Aller to account for microturbulence. This is, however, incorrect (Peters and Aller, 1970; Peters, private communication, 1970). On assuming a 4 km/sec microturbulent velocity, Peters and Aller derived SiII/SiIII and SII/SIII ionization balance temperatures different by less than 100^{o} from the results obtained for a zero velocity.

It is not possible to resolve these conflicting results here. It should be pointed out that the T_{eff} adopted for ι Her in the present study is in good agreement with the Hanbury Brown et al. temperature scale, with the Peters and Aller results and with the T_{eff} values derived by other workers from continuous energy distribution data. It is the viewpoint of the author that, if one cannot reproduce the observed continuum properties of a star with a given model atmosphere, then one cannot hope to interpret, in a physically meaningful way, the line spectrum of the star on the basis of that model atmosphere. Consequently, the extraordinarily low He/H ratio derived by Kodaira and Scholz for ι Her must be considered of doubtful validity.

V. PROJECTED ROTATIONAL VELOCITIES AND THE MG/H RATIO

Closely spaced lines, such as the MgII λ4481.13, .33 doublet, are clearly resolved in the spectra of γ Peg (Aller and Jugaku, 1958) and ι Her (Peters and Aller, 1970), which indicates V sin i values less than about 10 km/sec. Although the spectra of the five other stars of interest here are sharp-lined, one cannot resolve the MgII doublet in any of them. Thus, a quantitatively meaningful line profile analysis should take into account the possibility of a non-trivial rotational broadening contribution to their line shapes.

The V sin i estimates given in table 9 for 134 Tau, π Cet, HR 2154, HR 1861 and υ Ori were derived in the present study on the basis of a comparison between observed profiles of the MgII doublet and theoretical profiles calculated for a variety of assumed V sin i values (see section III). The MgII doublet profile is ideal for this purpose because its shape is rather sensitive to small variations in assumed V sin i and because it persists over the entire range of B spectral types. The observed MgII λ4481 profiles are given in table 8.

An interesting byproduct of this procedure was an estimate of the Mg/H abundance ratio for each of the stars considered. In each case it was possible to obtain an excellent theoretical match, in both core and wings, to the observed MgII profile with a suitable choice of V sin i

and Mg/H ratio. The V sin i value and Mg/H ratio so derived are virtually independent of each other, the former being determined by the profile shape, the latter being determined by the observed doublet strength.

The Mg/H ratios, given by number of atoms in table 9, are based upon a zero assumed most probable microturbulent velocity, V_T. The sensitivity of the derived Mg/H ratios to microturbulence decreases with increasing effective temperature - i.e. as the MgII doublet becomes weaker. An assumed $V_T \sim 5$ km/sec would reduce the Mg/H ratios derived for 134 Tau, π Cet and HR 2154 by more than a factor of three, but would have only a minor effect on the ratios obtained for υ Ori or HR 1861. Thus, it is noteworthy that the scatter from star to star in the derived Mg/H ratios is low and that only a slight, and possibly insignificant, trend toward smaller Mg/H ratios with increasing T_{eff} is obtained. Some of the scatter in the Mg/H ratios given in table 9 may be due to microturbulent broadening, but it seems unlikely that V_T values exceeding a few km/sec prevail, on the average, in the photospheres of these main-sequence stars. The V sin i values derived are quite insensitive to microturbulent broadening of the MgII doublet, as long as V_T remains $\lesssim 8$ km/sec.

The average magnesium abundance, log N(Mg)/N(H) + 12 = 7.8 ± 0.1, obtained here is slightly higher than the values 7.7 and 7.5 obtained by Hardorp and Scholz (1970) for λ Lep and τ Sco, respectively. Implicit in their analyses was an assumed $V_T \gtrsim 4$ km/sec. The estimate of the magnesium abundance of ι Her given in table 9 is substantially higher than that obtained by Kodaira and Scholz (1970) from the same line for the same star. This is remarkable in light of the fact that their adopted model atmosphere for ι Her is 1200° hotter in T_{eff} than the model utilized in the present study. One would expect an Mg/H ratio derived from the hotter model to be larger, not smaller, than the present value, since the MgII doublet decreases in strength with increasing T_{eff}.

VI. THE HeI PROFILES: RESULTS AND DISCUSSION

As discussed in section I, this investigation is concerned with finding that theoretical LTE HeI profile (and the corresponding He/H ratio) which most closely matches a given observed profile, at the effective temperature and surface gravity derived for the star in question. To this end, theoretical profiles for each of the eleven HeI lines listed in table 3 were computed, as outlined in section III, for a grid of model atmospheres, encompassing each combination of T_{eff} and log g listed in table 7, and for several choices of N(He)/N(H) (.05, .10, .15). Profiles

corresponding to other He/H ratios were interpolated from this set of computed profiles. The appropriate functions describing stellar rotational broadening (see section V) and instrumental broadening (see section II) were folded into each theoretical profile before it was compared to the observations.

The computations did not account explicitly for the blending of the HeI lines with lines of other elements. In most cases the HeI lines are sufficiently broad that such blends perturb only a small portion of the total observed profile. There are some notable exceptions, however. HeI λ5047.7 is seriously blended with either SII λ5047.3 or CII λ5047.2 or both over the entire spectral type range of interest; in the spectrum of υ Ori (B0) λ5047.7 is also blended with a line of undetermined identity at λ5048.1. The interpretation of HeI λ4921.9 is complicated by the blends with SiII λ4921.7 and with lines of FeII and SII at λ4923.9 throughout the middle B spectral types. At B0 and B1 OII λ4924.6 perturbs the red wing of HeI λ4921.9. OII lines at λ4120.6 and λ4121.5 seriously affect the profile of HeI λ4120.8 at spectral types earlier than B3. The blue wing of HeI λ4471.5 is virtually obliterated by a series of OII and NeII lines in early B type spectra and its core is blended with NeII λ4471.5. At spectral types later than B7, the blending of HeI λ4471.5 with FeII λ4472.9 becomes significant and HeI λ4026.2 becomes seriously

affected by FeII λ4024.6 and TiII λ4028.3. This is unfortunate since λ4026 and λ4471 are the only HeI lines which persist in sufficient strength to be well observed at B9. Blends of less importance are those of SII λ5014.0 with HeI λ5015.7 and of MgII $\lambda\lambda$4384.6, 4390.6 with HeI λ4387.9 in middle and late B spectra. No attempt has been made here to fit theoretical profiles to the observations in those cases where the total observed profile appears to be seriously influenced by blending.

The procedure of fitting theoretical to observed HeI profiles entailed the adjustment of the value of N(He)/N(H) assumed in the calculations until a good match was obtained in the line wings. Figures 1 through 6 illustrate the results for most (but not all) of the observed profiles considered. Each line is labeled with its central wavelength and with the value of N(He)/N(H) adopted in calculating the theoretical profile shown. In those cases where the observed wings could not be well matched for any choice of the He/H ratio (e.g. υ Ori, λ6678), the theoretical profile for N(He)/N(H) = 0.10 is illustrated for the sake of comparison. The continuum level for each profile is shown as a long horizontal line on the vertical axis nearest to the line in question. Residual flux scales (see equation 4) are labeled for a few of the lines on the left vertical axis of each diagram. Some of the more important blends are illustrated.

Figure 3 illustrates some of the HeI profiles for ι Her and γ Peg, the observations of which were drawn from other sources (see section II). Each HeI profile for ι Her, provided to the author by Mrs. Peters, varies rather markedly in shape among her three separate sets of observations. Moreover, each seems to be substantially underbroadened in the wings as compared to the theoretical predictions (see λ4121 and λ4438 profiles in figure 3). A rigorous profile analysis of ι Her was not possible because of the lack of reproducibility of the profile data at hand. The HeI equivalent widths given by Peters and Aller (1970) do seem to be reproducible from observation to observation, however. A rough estimate of the He/H ratio for ι Her will be made below, primarily on the basis of the latter data.

Table 10 lists, for most of the lines illustrated in figures 1 through 6, the ratio of the observed central depth in the line to the central depth of the LTE profile which most closely matches the line wings, viz.

$$\Delta = \frac{[\ 1 - R_\lambda(0)\ ]_{OBSERVED}}{[\ 1 - R_\lambda(0)\ ]_{LTE}} \qquad (10)$$

where R_λ is defined by equation 4. For a given line a scatter of $\pm$ 0.1 in this ratio, as determined from star to star, may be expected because of observational uncertainties. The central wavelengths in table 10 are listed in the approximate order of increasing photospheric depth of line core

formation, as indicated by the LTE contribution functions in the line (the contribution function in the line is defined as the integrand of the flux integral given by equation 1).

Inspection of figures 1 through 6 and table 10 leads to several conclusions:

1) It is not possible to match simultaneously an observed line core and the observed line wings with an LTE profile for most of the HeI lines considered at spectral types B1 and B0. The observed cores are systematically deeper and broader than predicted by the LTE calculations.
2) This problem seems to persist, for some HeI lines (λ4471, λ5876, λ6678 and perhaps also λ4388 and λ4026), over the entire range of spectral types considered (B0-B9).
3) Roughly speaking, the ratio of observed to computed central depths in the lines, Δ, decreases (approaches unity) with increasing depth of line formation in a given model atmosphere. At least for some lines ($\lambda\lambda$4471, 4026, 5016, 4388, 4121 and 4438) Δ remains approximately constant as a function of spectral type, except near B0 where it begins to increase.
4) The values of Δ given in table 10 for $\lambda\lambda$4438, 4121 and 4922 are consistent with those ratios derived theoretically by Poland (1970), although a rigorous

comparison is not possible at present. The values of Δ found here for λ4471 differ significantly from those given by Poland, the present values being larger near B0 ($T_{eff} \sim 30{,}000^{o}$) and smaller at later spectral types.

5) Agreement between the observed and predicted intensities of the forbidden components of λ 4026 and λ4388 is rather good in most cases. However, satisfactory theoretical fits to the forbidden components of λ4471 and λ4922 could not be obtained. In particular, the theoretical profiles of $\lambda\lambda$ 4471, 4922 predict too little absorption in the wavelength region between forbidden and allowed components. The displacements, $\Delta\lambda$, between the centers of the forbidden and allowed components of $\lambda\lambda$4471, 4922 observed here disagree with the predicted displacements by a few tenths of an angstrom in some cases. Finally, the center of the observed profile of forbidden λ4469.9 is slightly deeper than predicted for π Ceti and HR 1861 and is marginally shallower than predicted for γ Peg (the curious central reversal observed in λ4469.9 for HR 2154 is apparently not the result of a plate defect, but could be due to the presence of an unidentified blended line). Similar problems with these forbidden components have been encountered by Burgess and Cairns

(1970) in laboratory plasma studies of λλ4471, 4922, and by Snijders and Underhill (1970), in comparing the published theoretical λ4471 profiles of Shipman and Strom (1970) to observed profiles taken from the author's thesis (Leckrone, 1969) and from elsewhere in the literature. It is clear that currently available line broadening theories do not adequately describe the regions near the forbidden components of λ4471 and λ4922.

A comment is in order with regard to conclusion 2) above. In the spectrum of 134 Tau (B9), the coolest star considered here, the observed wings of λ4026 and λ4922 are perturbed by the presence of blends and, moreover, are too weak to be observed with great precision. The observed core of λ4023 can be well matched with a theoretical profile calculated for N(He)/N(H) ~ 0.13. However, it is not possible to match the observed core of λ4471 at any He/H ratio less than 0.19, at the adopted T_{eff} and log g (see figure 6). This latter value is much higher than the He/H ratio derived from the wings of λ4471 for any other star observed. In addition, the difference between the He/H ratio derived for 134 Tau with λ4026 and that found with λ4471 is much greater than the corresponding differences found for the other stars. Slight changes in assumed T_{eff} and log g will alter the He/H ratios derived from both lines but will not close the gap between them. It is tempting to speculate that the core of λ4471 has been deepened in 134 Tau

by the same physical processes which produce the great observed central depth of this line in the hotter stars investigated here. If this is true, then the hypothesis that such lines can be described in LTE when they are weak, as in the spectra of the latest B stars (see for example the discussion by Underhill, 1966) is incorrect.

Table 11 summarizes the author's best estimates of the N(He)/N(H) values, derived primarily from analyses of the weaker HeI lines and the wings of the stronger lines. Each abundance estimate is coded a, b, c or d depending upon how it was obtained. "a" indicates a good theoretical fit to both core and wings of a line (usually relatively weak); "b" indicates that only the line wings could be fit; "c" denotes a rough fit to observed profiles of relatively low quality or to observed profiles strongly perturbed by blends; "d" indicates an abundance derived from equivalent width data alone. The He/H ratio obtained from an individual line is given to three decimal places, the first two of which are significant.

Shipman and Strom (1970) have suggested that accurate He/H ratios can be determined in general with LTE calculations, from low-dispersion spectra, where only the equivalent width of λ4471 may be accurately measured. A difficulty with this general approach is illustrated in table 12, where N(He)/N(H) values derived from the equivalent widths of λ4471

are compared to abundances derived from the wings of the corresponding λ4471 profiles for the stars investigated here. Within the framework of the LTE assumption, both wing profiles and equivalent widths of λ4471 yield approximately the same He/H ratios in the spectral type range B5-B2. In this range the λ4471 line reaches its maximum strength and the line core makes a relatively small contribution to the line equivalent width. However, Shipman and Strom's conjecture clearly does not hold at spectral types later than B5 or earlier than B2. In the cases of υ Ori, HR 1861, π Ceti and possibly 134 Tau, the observed λ4471 equivalent widths yield substantially higher He/H ratios than those derived from the wings of the line profiles. In this respect the present empirical results disagree with the conclusion of Poland (1970), that the deepening of HeI line cores by non-LTE effects has a negligible influence on the line equivalent widths and on abundances derived therefrom.

One can expect that the He/H ratios derived from the observed HeI equivalent widths for ι Her, as listed in table 11, are roughly comparable to the values one would obtain from high quality profile data for this star, because it lies in the B5-B2 spectral type range. Nevertheless, the results obtained for this star should be given rather low weight.

No striking systematic effects were noted in He/H ratios derived from HeI singlet lines as opposed to those obtained

for lines arising from the triplet levels. Figure 7 illustrates observed and theoretically predicted singlet/triplet equivalent width ratios, for the stars investigated, plotted as a function of spectral type. The $\lambda 4438/\lambda 4713$ ($2^1P\text{-}5^1S/2^3P\text{-}4^3S$) ratio illustrates the trend for relatively weak, sharp series lines. The trend for strong hydrogenic lines is illustrated by the ratio $\lambda 4388/\lambda 4026$ ($2^1P\text{-}5^1D/2^3P\text{-}5^3D$). A value of N(He)/N(H) = 0.10 has been assumed in figure 7 and the calculated equivalent widths were truncated in the wings as follows: $\lambda 4438 \pm 1.0$Å, $\lambda 4713 \pm 1.3$Å, $\lambda 4388 \pm 4$Å, $\lambda 4471 \pm 6$Å. The observational uncertainty in the measured singlet/triplet ratios is typically about $\pm$ 0.07. The calculations reproduce the observed singlet/triplet trends, both qualitatively and quantitatively, to within the uncertainty of the observations. $\lambda 4026$ yielded a lower than average N(He)/N(H) value for five of the six stars listed in table 11, due possibly to a systematic effect in the broadening theory for this line. That the observed $\lambda 4388/\lambda 4026$ ratios are systematically higher than predicted near the peak of the curve illustrated in figure 7 is a partial consequence of this effect.

On the basis of the results discussed above, it appears that one need not invoke a decoupling of singlet and triplet level populations (e.g. Struve and Würm, 1938) to explain the observed trends in the singlet/triplet equivalent width ratios for main sequence B stars. In fact, the observed trends can be

reproduced, at least qualitatively, with LTE calculations in spite of evident deviations from LTE in the line cores. They are due apparently to "curve-of-growth" effects of the sort first postulated by Goldberg (1939). These results are consistent with the conclusions of recent studies by Norris (1970) and Poland (1970). Neither the present results nor those of Norris and Poland preclude the possibility of a decoupling of singlet and triplet populations in giant or supergiant B star photospheres, however.

The assumption of a 5 km/sec microturbulent velocity, V_T, produces a negligible effect on abundances derived from a very weak line, such as HeI λ4438, or on abundances obtained from the wings of a strong line, such as HeI λ4471. It does, however, influence significantly the abundances derived from such lines as HeI λ4121, 4713, or 5016 in most cases. Comparable He/H ratios were found for all of these lines, as listed in table 11. The absence of systematic weak line-strong line trends in the helium abundances derived here indicates that the assumption of zero microturbulence in these calculations was justified (see sections III and V).

The average value of N(He)/N(H), listed for a given star at the bottom of table 11, is based upon all of the lines for which estimates of the He/H ratio could be made, regardless of their quality. In general, each average differs by no more than 0.005 from the average one obtains by

exclusive use of the highest quality data (coded "a" or "b" in table 11). Table 11 also gives, for each star, the formal mean error in the value of N(He)/N(H) determined from a single line (σ) and the formal mean error in the average stellar He/H ratio obtained ($\sigma/\sqrt{N}$, where N is the number of lines utilized).

The small scatter in the He/H ratios derived from line to line for a given star and the small scatter in the averages derived from star to star attest to the quality of the observations and the internal consistency of the analyses. However, the formal mean errors in the average He/H ratios listed are probably unrealistically small because they do not account for the effects of possible systematic errors. Principal among these are the uncertainties in the calibration of the spectrophotometric data utilized in deriving stellar T_{eff} values; the uncertainties in the line broadening theory for the HI lines used in estimating log g for each star; uncertainties in the Stark broadening calculations for the HeI lines themselves; and the uncertain effect of possible deviations from LTE level populations in those deep atmospheric regions where the weak HeI lines and the wings of the strong lines are formed.

The stellar He/H ratios given in Table 11 are fundamentally linked to the effective temperatures derived from spectrophotometric data reduced to the standard system defined

by Oke and Schild (1970). Table 13 compares the average N(He)/N(H) values so derived to approximate values obtained from similar analyses, based upon effective temperatures derived within the context of Hayes' (1970) standard system. The pertinent T_{eff} and log g values may be found in table 7. The adoption of the effective temperatures associated with Hayes' standard system results in a systematic increase in derived He/H ratios with decreasing T_{eff}. It should be noted that the sensitivity of the HeI lines to small errors in assumed T_{eff} also increases with decreasing T_{eff}. Moreover, the scatter from line to line in the abundances derived for π Ceti and HR 2154 increases markedly when the Hayes system is adopted. The good internal consistency of the results obtained on the Oke-Schild system weighed strongly in the author's decision to adopt these results in developing the primary conclusions of this paper.

As noted in section IV, use of the Kolb-Griem Stark broadening theory for H_γ and H_δ would have resulted in estimates of stellar log g values lower by about 0.2 than those derived here on the basis of the formalism of Edmonds et al. The assumption of the lower log g values alters the average He/H ratios derived for π Ceti, HR 2154 and ι Her by less than .003. However, it will result in an increase in the estimated average N(He)/N(H) values for γ Peg, HR 1861 and υ Ori by an amount $\leq$ 0.015. Thus, the effect of this uncertainty in the adopted stellar surface gravities on the overall average He/H ratio quoted below for the six stars cannot be ignored.

Except for the case of HR 2154, the wings of the hydrogenic HeI lines of each star yielded an average He/H ratio lower by about 0.015 than the average obtained from the isolated HeI lines for that star. In addition, as pointed out above, λ4026 tended to yield systematically lower N(He)/N(H) estimates than those obtained from any other line. These small discordances may reflect systematic errors in the Stark broadening functions utilized. A reasonable estimate of the uncertainty in the average N(He)/N(H) derived for each star, from both isolated and hydrogenic lines, due to possible systematic errors in the line broadening data used is $\pm$ 0.01.

Within the context of the LTE analyses discussed in this paper, the best estimate that can be made of the average helium abundance for the photospheres of the six stars considered is N(He)/N(H) = .106. This average is based upon all 46 lines for which He/H ratios are listed in table 11. When only those 28 lines coded "a" or "b" in table 11 are utilized, the average derived is .105. It is unlikely that systematic errors in the adopted stellar effective temperatures and surface gravities or in the adopted line broadening functions could cause the average He/H ratio for these stars to fall outside of the range 0.095-0.125. It seems safe to conclude that there exists little natural scatter in the photospheric He/H ratio among the stars considered.

All of these stars are nearby members of the Orion spiral arm. According to Sharpless (1952), two of them (υ Ori and HR 1861) are members of the Orion association. It is encouraging that the He/H ratios obtained in the present study for these two stars (0.099 and 0.108, respectively) are in close agreement with the results of recent optical studies of the Orion nebula. Peimbert and Costero (1969) find an average N(He)/N(H) = 0.104 for three observed positions in this nebula. Comparable values have been found for a number of galactic and extra-galactic HII regions by Piembert and Costero and by Piembert and Spinrad (1970), so that excellent agreement now obtains between He/H ratios derived from optical HII region observations in general and those determined in the present study of stellar spectra. The average N(He)/N(H) value derived here is also in substantial agreement with the average result (N(He)/N(H) = $0.12 \pm {}^{.015}_{.025}$) obtained by Popper et al. (1970) from eclipsing binary masses and luminosities.

The present results are slightly higher than the average value, $N(He^+)/N(H^+) = .089 \pm .009$, obtained from observations of radio recombination lines of twelve "Group I" HII regions, as recently discussed by Churchwell (1970). This difference may not be significant, however, and in any event could be completely resolved if a rather

small fraction of the helium present in the HII regions considered were in the neutral state. However, some high excitation HII regions, observed at radio wavelengths, appear to have He/H ratios substantially lower than the value quoted above. Indeed, helium recombination lines cannot be detected at all for a few of them (e.g. Mezger and Churchwell, 1970; Churchwell, 1970). Also puzzling are the solar cosmic ray observations of Durgaprasad et al. (1960), which yield an estimated $N(He)/N(H) = 0.06 \pm 0.01$. Clearly, the discordance between these latter He/H ratio estimates and those obtained from stellar spectroscopy, from optical spectroscopy of HII regions and from the eclipsing binary solutions must be resolved before one can consider the characteristic helium content of population I objects to be well established.

The question of the physical significance of the helium abundances derived in the present study must ultimately rest on a rigorous test of the LTE assumption for the atmospheric regions where the weaker HeI lines and the wings of the strong HeI lines are formed. It is hoped that the observations and LTE calculations included here will provide a useful framework within which such a test may be carried out.

VII. CONCLUSIONS

Theoretical profiles of the HeI lines, calculated on the assumption of LTE, do not, in many cases, adequately describe the corresponding observed profiles, taken from high resolution stellar spectra. Usually the weaker HeI lines and the wings of the strong lines can be matched, but the cores of the strong lines are observed to be systematically deeper and broader than predicted. This problem seems to persist over the entire range of B spectral types. The exclusive use of HeI equivalent width data, without reference to the corresponding line profiles, in the estimation of He/H ratios, is acceptable in certain specific cases, but is not legitimate as a general procedure.

He/H ratios, estimated by use of the weaker HeI lines and the strong line wings, average 0.106, by number of atoms, for six stars investigated. There appears to be virtually no natural scatter in photospheric He/H ratio among these stars.

Use of the Hayes (1970) standard calibration of Vega in estimating stellar T_{eff} values leads to systematic variations in the derived He/H ratios, as a function of spectral type; these trends vanish when the Oke-Schild (1970) standard calibration is adopted. The hydrogenic HeI lines investigated yield estimated He/H ratios which are systematically less, by a small amount, than those obtained from

the isolated HeI lines, for five of the six stars considered. This may indicate the presence of small systematic errors in the currently available Stark broadening functions. Currently available Stark broadening data do not adequately describe the forbidden components of HeI λ4471 and λ4922. It is unlikely that systematic errors in the adopted stellar effective temperatures or surface gravities or in the line broadening data utilized could force the average derived He/H ratio for these six stars to fall outside the range 0.095-0.125.

Comparable He/H ratios are obtained from singlet and triplet HeI lines, which indicates that the singlet and triplet level populations are not decoupled in the deep atmospheric regions where the weak HeI lines and the strong line wings are formed. The observed variations in singlet/triplet equivalent width ratios, as a function of spectral type, are well reproduced by the LTE calculations in spite of evident deviations from LTE in the line cores.

Acknowledgements: Unless otherwise noted, the observational materials contained in this paper were taken from a dissertation, submitted to the University of California at Los Angeles, in partial fulfilment of the requirements for the degree of Doctor of Philosophy.

I would like to extend special thanks to Professor Lawrence H. Aller for his continued guidance and support. The many stimulating discussions and the valuable advice provided by Professor Daniel M. Popper are also gratefully acknowledged. I am indebted to John P. Oliver for his assistance with regard to the observational programs related to this research.

References

Adams, T.F., Morton, D.C. 1968, Ap.J. 152, 195.

Aller, L.H. 1956, The quantitative chemical analysis of early-type stars in Vistas in Astronomy, Volume Two, Ed. A. Beer, Pergamon Press, New York, p. 1284.

Aller, L.H. 1963, The Atmospheres of the Sun and Stars. Ronald Press, New York.

Aller, L.H., Jugaku, J. 1958, Ap.J. 127, 125.

Aller, L.H., Jugaku, J. 1959, Ap.J. Suppl. 4, 109.

Aller, L.H., Ross, J.E. 1967, Spectroscopic Analyses of A and B Stars of Peculiar Composition in The Magnetic and Related Stars, Ed. R.C. Cameron, Mono Book Corp. Baltimore, p. 339.

Bahcall, J.N., Ulrich, R.K. 1970, Ap.J. 160, L57.

Bahner, K. 1963, Ap.J. 138, 1314.

Barnard, A.J., Cooper, J., Shamey, L.H. 1969, Astr.Astrophys. 1, 28.

Baschek, B., Norris, J. 1970, Ap.J. Suppl. 19, 327.

Bradley, P.T., Morton, D.C. 1969, Ap.J. 156, 687.

Brown, R. Hanbury, Davis, J., Allen, L.R., Rome, J.M. 1967, M.N.R.A.S. 137, 393.

Burgess, D.D., Cairns, C.J. 1970, J. Phys.(B) 3, L67.

Churchwell, E. 1970, thesis, Indiana University.

Code, A.D. 1960, Stellar Energy Distribution in Stellar Atmospheres, Ed. J.L. Greenstein, Univ. Chicago Press, Chicago, p. 50.

Durgaprasad, N., Fichtel, C.E., Guss, D.E., Reames, D.V. 1968, Ap.J. 154, 307.

Edmonds, F.N., Schlüter, H., Wells, D.C. 1967, Mem. R.A.S. 71, 271.

Finn, G.D., Mugglestone, D. 1965, M.N.R.A.S. 129, 221.

Fischel, D. 1963, thesis, Indiana University.

Goldberg, L. 1939, Ap.J. 89, 623.

Griem, H.R. 1964, Plasma Spectroscopy. McGraw-Hill, New York

Griem, H.R. 1968, Ap.J. 154, 1111.

Griem, H.R., Baranger, M., Kolb, A.C., Oertel, G. 1962, Phys. Rev. 125, 177.

Hardorp, J., Scholz, M. 1970, Ap.J. Suppl. 19, 193.

Hayes, D.S. 1970, Ap.J. 159, 165.

Henry, R.C., Mihalas, D. 1964, Ap.J. 140, 873.

Hickock, F.R., Morton, D.C. 1968, Ap.J. 152, 203.

Hoffleit, D. 1964, Catalogue of Bright Stars. Yale Universit Observatory, New Haven.

Hummer, D.G., Mihalas, D. 1967, Ap.J. 150, L57.

Hunger, K., Klinglesmith, D.A. 1969, Ap.J. 157, 721.

Hyland, A.R. 1967, thesis, Australian National University.

Jager, C. De, Neven, L. 1960, B.A.N. 15, 55.

Johnson, H.L., Mitchell, R.I., Iriarte, B., Wisniewski, W.Z. 1966, Commun. Lunar Planet. Lab. 4, 99.

Johnson, H.R., Poland, A.I. 1969, J.Q.S.R.T. 9, 1151.

Jugaku, J. 1957, thesis, University of Michigan.

Jugaku, J. 1959, Publ. Astr. Soc. Japan, 11, 161.

Jugaku, J., Sargent, W.L.W. 1968, Ap.J. 151, 259.

Klinglesmith, D.A. 1970, NASA Sp. Publ. (in press).

Kodaira, K., Scholz, M. 1970, Astron.Astrophys. 6, 93.

Leckrone, D.S. 1969, thesis, University of California, Los Angeles.

Mezger, P.G., Churchwell, E. 1970, Bull.A.A.S. (abstract in press; paper delivered at 132nd meeting of A.A.S., Boulder, Colorado).

Mihalas, D. 1964, Ap.J. 140, 885.

Mihalas, D. 1965, Ap.J. Suppl. 9, 321.

Mihalas, D. 1967a, The Calculation of Model Stellar Atmospheres in Methods in Computational Physics, Volume 7, Eds. B. Alder, S. Fernbach, M. Rotenberg, Academic Press, New York, p. 1.

Mihalas, D. 1967b, Ap.J. 149, 169.

Mihalas, D., Morton, D.C. 1965, Ap.J. 142, 253.

Mihalas, D., Auer, L.H. 1970, Ap.J. 160, 1161.

Norris, J. 1970, Ap.J. Suppl. 19, 337.

Norris, J., Baschek, B. 1970, Ap.J. Suppl 19, 305.

Oke, J.B. 1965, A. Rev. Astr. Astrophys. 3, 23.

Oke, J.B., Schild, R.E. 1970, Ap.J. 161, 1015.

Peimbert, M., Costero, R. 1969, Bol. Obs. Tonantzintla y Tacubaya, 5, 3.

Peimbert, M., Spinrad, H. 1970, Ap.J. 159, 809.

Peters, G.J., Aller, L.H. 1970, Ap.J. 159, 525.

Poland, A.I. 1970, Ap.J. 160, 609.

Popper, D.M., Jørgensen, H.E., Morton, D.C., Leckrone, D.S. 1970, Ap.J. 161, L57.

Sharpless, S. 1952, Ap.J. 116, 251.

Shipman, H.L., Strom, S.E. 1970, Ap.J. 159, 183.

Slettebak, A. 1954, Ap.J. 119, 146.

Slettebak, A., Howard, R.F. 1955, Ap.J. 121, 102.

Snijders, M.A.J., Underhill, A.B. 1970, M.N.R.A.S. (in press).

Ström, S.E., Peterson, D.M. 1968, Ap.J. 152, 859.

Struve, O., Würm, K. 1938, Ap.J. 88, 84.

Tayler, R.J. 1967, Q.J.R.A.S. 8, 313.

Traving, G. 1955, Z. Astrophys. 36, 1.

Traving, G. 1957, Z. Astrophys. 41, 215.

Underhill, A.B. 1953, J.R.Astr. Soc.Can. 47, 153.

Underhill, A.B. 1966, The Early Type Stars. D. Reidel Publ. Co. Dordrecht, Holland.

Underhill, A.B., Waddell, J.H. 1959, Nat. Bur. Stand. Cir. No. 603.

Unsöld, A. 1955, Physik der Sternatmosphären. Springer-Verlag, Berlin, p. 508.

Vardya, M.S. 1964, Ap.J. Suppl. 8, 277.

Van Citters, G.W., Morton, D.C. 1970, Ap.J. 161, 695.

Wampler, E.J. 1966, Ap.J. 144, 921.

Wiese, W.L., Smith, M.W., Glennon, B.M. 1966, Atomic Transition Probabilities. U.S. Government Printing Office, Washington.

Wolff, S.C., Kuhi, L.V., Hayes, D. 1968, Ap.J. 152, 871.

CAPTIONS FOR FIGURES

Fig. 1. Observed (xxx) and theoretical LTE (———) HeI profiles for υ Orionis (B0 V). Profiles are plotted in units of residual flux, R_λ, as a function of displacement from the line center, $\Delta\lambda$(Å). The continuum level for each profile is shown as a long horizontal mark on the vertical axis nearest to the line in question. Residual flux scales are labeled only for a few of the lines on the left vertical axis. Each line is labeled with its central wavelength and the value of N(He)/N(H) adopted in calculating the theoretical profile shown. Some of the more important blends are illustrated. A similar format applies to figures 2-6.

Fig. 2. Observed (xxx) and theoretical LTE (———) HeI profiles for HR 1861 (B1 V). See caption for figure 1.

Fig. 3. Observed (xxx) and theoretical LTE (———) HeI profiles for γ Pegasi (B2 V) and ι Herculis (B3 V). See caption for figure 1.

Fig. 4. Observed (xxx) and theoretical LTE (———) HeI profiles for HR 2154 (B5 IV). See caption for figure 1.

Fig. 5. Observed (xxx) and theoretical LTE (———) HeI profiles for π Ceti (B7 V). See caption for figure 1.

Fig. 6. Observed (xxx) and theoretical LTE (———) HeI profiles for 134 Tauri (B9 IV). See caption for figure 1.

Fig. 7. Observed (xxx) and theoretically predicted (———) singlet/triplet equivalent width ratios, plotted as a function of spectral type. The calculations assume N(He)/N(H) = 0.10.

Table 1. Data for the stars investigated

Star	HD	Sp	V	B-V	U-B	Published V sin i (km/sec)	Instrumental Systems (Table 2)
134 Tauri	38899	B9 IV	4.91	-0.07	-0.16	8	1,3
π Ceti	17081	B7 V	4.25	-0.14	-0.45	15	1,3
HR 2154	41692	B5 IV	5.38	-0.13	-0.54	10	2,3
ι Herculis	160762	B3 V	3.80	-0.18	-0.69	0	
γ Pegasi	886	B2 IV	2.83	-0.23	-0.86	0	
HR 1861	36591	B1 V	5.35	-0.19	-0.93	20	2,3
υ Orionis	36512	B0 V	4.62	-0.26	-1.07	10	1,3

Table 2. Characteristics of the spectroscopic instrumental systems

System No.	1	2	3
Camera Focal Length (meters)	4.06	2.03	1.02
Collimator Focal Length (meters)	6.10	6.10	6.10
Slit Width (microns)	40	70	135
Dispersion (Å/mm)	2	4	8
Plate Type	IIaO baked	IIaO baked	IIaF + GG11 filter
Wavelength Range (Å)	3560-4780	3590-4810	4760-6380 5174-6800
Resolution (Å)	.05	.09	.24

Table 3. Data for the HeI lines considered

Transition	Central Wavelength(Å)	f-value	Statistical Weight	Excitation Potential (e.v.)	Comments
2^3P-5^3F	4025.5		9	20.958	forbidden
2^3P-5^3D	4026.2	0.0474	9	20.958	
2^3P-5^3S	4120.8	0.00365	9	20.958	
2^1P-5^1F	4387.4		3	21.212	forbidden
2^1P-5^1D	4387.9	0.0436	3	21.212	
2^1P-5^1S	4437.6	0.00308	3	21.212	
2^3P-4^3F	4469.9		9	20.958	forbidden
2^3P-4^3D	4471.5	0.125	9	20.958	
2^3P-4^3S	4713.2	0.0118	9	20.958	
2^1P-4^1F	4920.4		3	21.212	forbidden
2^1P-4^1D	4921.9	0.122	3	21.212	
2^1S-3^1P	5015.7	0.1514	1	20.610	
2^1P-4^1S	5047.7	0.00834	3	21.212	
2^3P-3^3D	5875.7	0.609	9	20.958	
2^1P-3^1D	6678.2	0.711	3	21.212	

Table 4. Observed spectral energy distributions given in the form $-2.5 \log F_\nu$ + const., normalized to $m_\nu = 0.0$ at $\lambda 5556$

λ(Å)	134 Tauri	HR 2154
3300	+ .792	+ .132
3350	+ .769	+ .128
3400	+ .781	+ .125
3450	+ .761	+ .133
3500	+ .662	+ .144
3571	+ .694	+ .169
3636	+ .699	+ .169
3704	+ .704	+ .190
4032	- .360	- .382
4167	- .352	- .353
4255	- .340	- .341
4464	- .283	- .281
4566	- .271	- .278
4786	- .212	- .231
5000	- .157	- .166
5263	- .086	- .094
5556	.000	.000
5840	+ .051	+ .043
6056	+ .103	+ .129
6436	+ .190	+ .206
6790	+ .256	+ .274
7100	+ .313	+ .340
7550	+ .393	+ .418

Table 5. Observed Hγ profiles in residual flux units

$\Delta\lambda$ (Å)	HR 2154	HR 1861
0.0	.325	.438
1.0	.515	.633
2.0	.624	.713
3.0	.696	.778
4.0	.761	.836
5.0	.814	.879
6.0	.860	.903
7.0	.890	.923
8.0	.913	.938
9.0	.925	.948
10.0	.941	.957
11.0	.951	.966
12.0	.959	.971
13.0	.968	.978
14.0	.973	.983
15.0	.977	.986
16.0	.980	
17.0	.982	

Table 6. Observed Hδ profiles in residual flux units

Δλ(Å)	134 Tauri	π Ceti	HR 2154	HR 1861	υ Orionis
0.0	.200	.253	.343	.461	.495
1.0	.306	.404	.490	.633	.620
2.0	.371	.488	.593	.707	.720
3.0	.431	.564	.668	.779	.798
4.0	.486	.634	.733	.831	.852
5.0	.544	.695	.780	.874	.887
6.0	.594	.748	.828	.906	.914
7.0	.647	.789	.870	.928	.938
8.0	.688	.823	.900	.943	.955
9.0	.731	.852	.922	.951	.965
10.0	.767	.876	.937	.961	.975
11.0	.796	.896	.951	.969	.980
12.0	.824	.912	.961	.974	.986
13.0	.853	.926	.970	.979	
14.0	.869	.938	.974	.983	
15.0	.887	.947	.976	.986	
16.0	.901	.956	.980		
17.0	.916	.963	.983		
18.0	.924	.969			
19.0	.932	.971			
20.0	.945	.973			
21.0	.955	.976			
22.0	.960	.979			
23.0	.968	.980			
24.0	.972				

Table 7. Stellar effective temperatures and surface gravities derived with spectrophotometric data reduced to two different standard systems and with reddening-independent Q

	Oke-Schild System		Hayes System		Q	
Star	T_{eff}	log g	T_{eff}	log g	T_{eff}	log g
134 Tauri	10,700°	4.0	10,400°	3.9		
π Ceti	13,500°	3.8	13,100°	3.7		
HR 2154	15,100°	3.4	14,400°	3.3		
ι Herculis	17,500°	4.0	17,000°	4.0	17,900	4.1
γ Pegasi	21,900°	4.1	20,600°	3.9	20,700°	3.9
HR 1861					24,800°	4.0
υ Orionis	31,000°	4.3	28,600°	4.0	31,300°	4.3

Table 8. Observed MgII λ4481 profiles in residual flux units

Δλ(Å)	134 Tauri	π Ceti	HR 2154	HR 1861	υ Orionis
-1.0					
-0.9	.992				
-0.8	.977	.988			
-0.7	.961	.982	.990		
-0.6	.940	.976	.971	1.000	1.000
-0.5	.908	.948	.924	.998	.981
-0.4	.799	.888	.847	.976	.947
-0.3	.712	.751	.781	.926	.923
-0.2	.591	.632	.719	.835	.883
-0.1	.521	.478	.668	.757	.845
0.0	.489	.406	.636	.731	.841
+0.1	.513	.479	.656	.763	.846
+0.2	.609	.629	.714	.832	.882
+0.3	.712	.786	.776	.937	.930
+0.4	.801	.918	.851	.983	.954
+0.5	.900	.959	.924	.995	.974
+0.6	.932	.977	.974	1.000	.992
+0.7	.948	.986			1.000
+0.8	.968	.991			
+0.9	.985				
+1.0					

Table 9. Derived stellar projected rotational velocities and magnesium abundances

Star	V sin i (km/sec)	N(Mg)/N(H)	log N(Mg)/N(H) + 12
134 Tauri	24	6.2×10^{-5}	7.79
π Ceti	13	8.5×10^{-5}	7.93
HR 2154	28	7.5×10^{-5}	7.88
ι Herculis		4.7×10^{-5}	7.67
γ Pegasi		6.7×10^{-5}	7.83
HR 1861	15	5.4×10^{-5}	7.73
υ Orionis	25	5.8×10^{-5}	7.76

Table 10. Ratios of observed to calculated profile central depths (Δ) for the stars investigated; lines listed in approximate order of increasing atmospheric depth of core formation

λ	134 Tauri	π Ceti	HR 2154	γ Pegasi[a]	HR 1861	υ Orionis
5876		1.37	1.69	1.13	1.56	1.88
6678				1.52	1.83	2.11
4471	> 1.19	1.20	1.07	1.21	1.23	1.42
4922					1.31	
4026	> 1.04	1.08	1.04	1.15	1.17	1.37
5016		1.00	1.00	1.00	1.21	1.36
4713		.85				.95
4388		1.22	.98	1.25	1.19	1.31
4121		.94	1.13	1.04		
4438		1.00	1.08		1.11	1.14

a - instrumental broadening not accounted for

Table 11. Derived He/H ratios by number of atoms

λ	π Ceti	HR 2154	ι Herculis	γ Pegasi	HR 1861	υ Orionis
4026	.087 b	.121 b	.089 d	.084 b	.086 b	.087 b
4121	.115 a	.091 a	.122 c	.154 d		
4388	.098 b	.133 a	.108 d	.095 b	.115 b	.092 b
4438	.120 a	.097 a	.126 c	.095 d	.100 c	.107 a
4471	.114 b	.107 b	.102 d	.093 b	.107 b	.088 b
4713	.116 c		.100 c	.082 d		.126 a
4922	.109 c		.100 d	.112 d	.108 b	
5016	.125 a	.121a		.108 d		.100 c
5876		.110 b		.100 b	.120 c	.090 b
6678				.122 b	.120 c	
⟨N(He)/N(H)⟩	.110	.111	.107	.104	.108	.099
σ	.012	.015	.013	.021	.012	.014
$\sigma/\sqrt{N}$	.004	.006	.005	.007	.005	.005

Key:

a - good fit to line core and wings

b - good fit to line wings only

c - rough fit to low quality observed profile or to profile strongly influenced by blends

d - derived from equivalent width data only

Table 12. N(He)/N(H) values derived from λ4471 wing profiles compared to values derived from λ4471 equivalent widths

Star	Sp	λ4471 wing profile Results	λ4471 Equivalent Width Results
134 Tauri	B9		~ .19
π Ceti	B7	.114	.156
HR 2154	B5	.107	.114
ι Herculis	B3		.102
γ Pegasi	B2	.093	.103
HR 1861	B1	.107	.187
υ Orionis	B0	.088	> .20

Table 13. N(He)/N(H) values derived with effective temperatures determined relative to Oke-Schild calibration of Vega compared to approximate values derived when Hayes' calibration of Vega is used

Star	Sp	Results with Oke-Schild System	Results with Hayes System
π Ceti	B7	.110	.14
HR 2154	B5	.111	.14
ι Herculis	B3	.107	.12
γ Pegasi	B2	.104	.11
HR 1861	B1	.108	
υ Orionis	B0	.099	.10

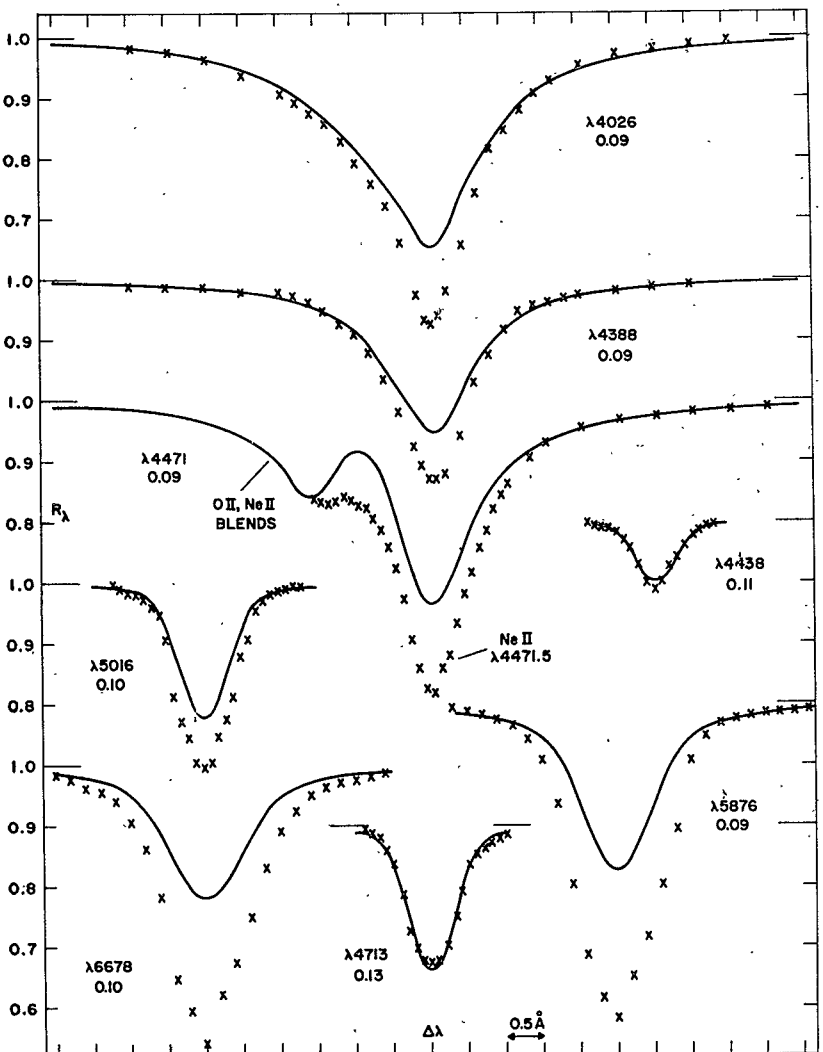
λ4026
0.09
λ4388
0.09
λ4471
0.09
O II, Ne II
BLENDS
R_λ
λ4438
0.11
Ne II
λ4471.5
λ5016
0.10
λ5876
0.09
λ6678
0.10
λ4713
0.13
Δλ
0.5 Å

FIGURE 1

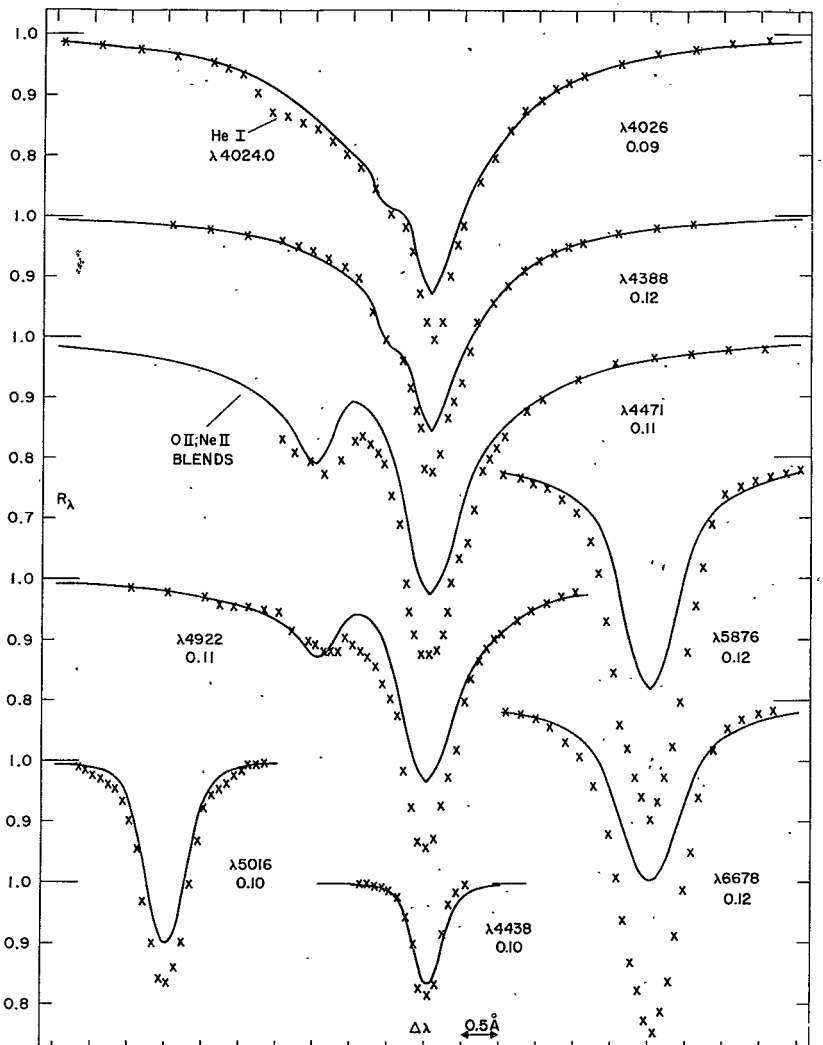
He I
λ4024.0
λ4026
0.09
λ4388
0.12
O II;Ne II
BLENDS
λ4471
0.11
R_λ
λ4922
0.11
λ5876
0.12
λ5016
0.10
λ4438
0.10
λ6678
0.12
Δλ
0.5Å
1.0
0.9
0.8
0.7

FIGURE 2

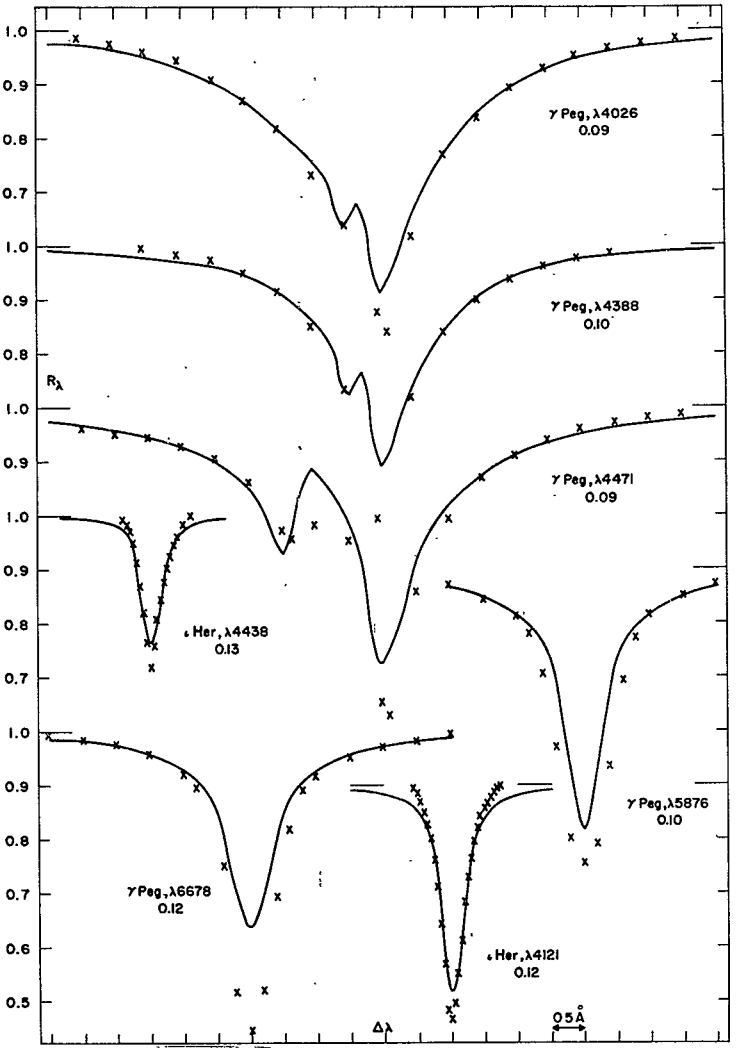
γ Peg, λ4026
0.09
γ Peg, λ4388
0.10
R_λ
γ Peg, λ4471
0.09
ε Her, λ4438
0.13
γ Peg, λ5876
0.10
γ Peg, λ6678
0.12
ε Her, λ4121
0.12
0.5Å
Δλ

FIGURE 3

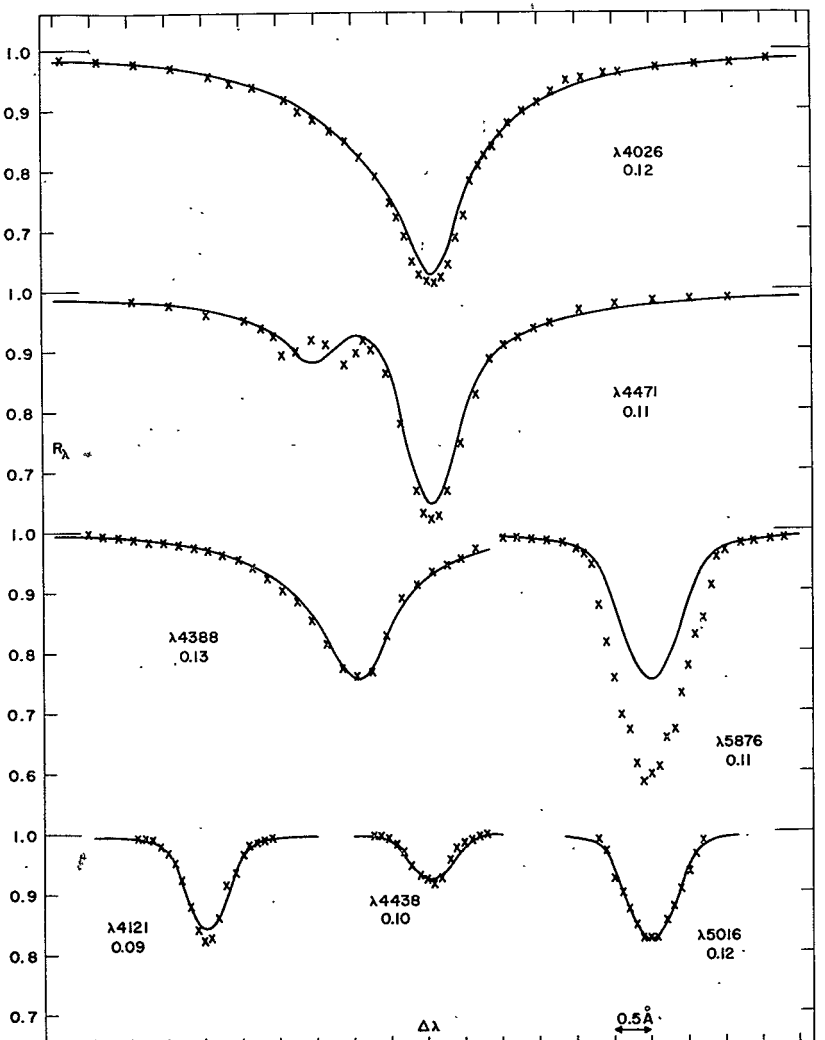
1.0
0.9
0.8
0.7
λ4026
0.12
λ4471
0.11
R_λ
λ4388
0.13
λ5876
0.11
0.6
λ4121
0.09
λ4438
0.10
λ5016
0.12
Δλ
0.5Å

FIGURE 4

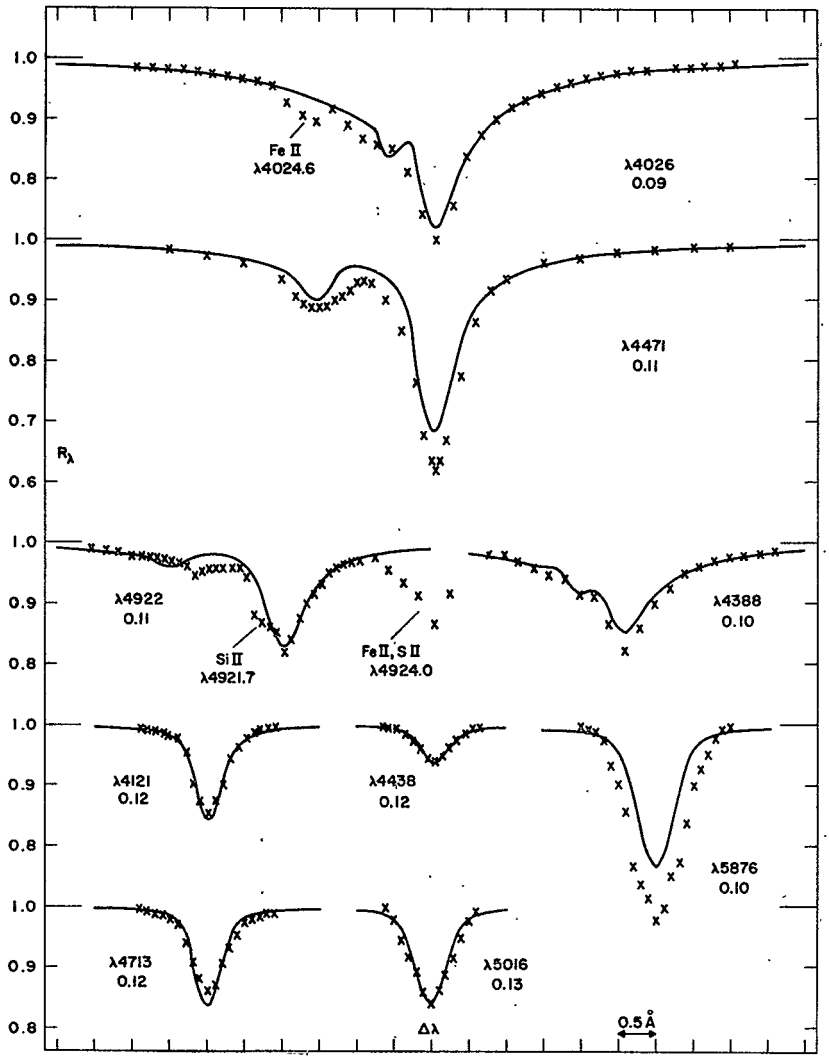
Fe II
λ4024.6
λ4026
0.09
λ4471
0.11
R_λ
λ4922
0.11
Si II
λ4921.7
Fe II, Si II
λ4924.0
λ4388
0.10
λ4121
0.12
λ4438
0.12
λ5876
0.10
λ4713
0.12
λ5016
0.13
Δλ
0.5 Å

FIGURE 5

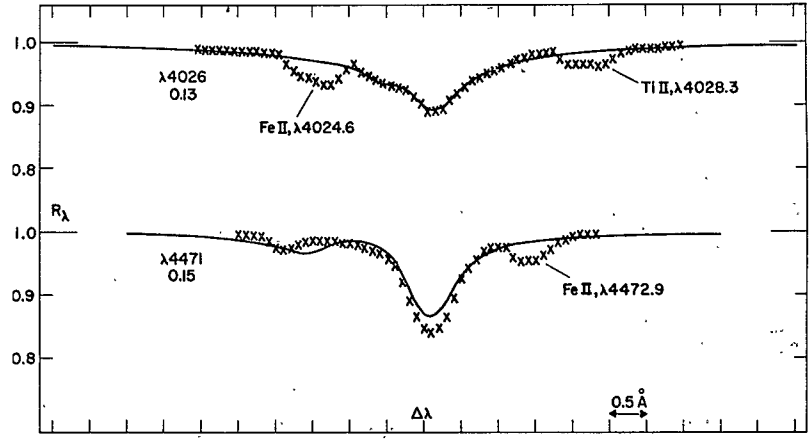
1.0
0.9
0.8
λ4026
0.13
Fe II, λ4024.6
Ti II, λ4028.3
R_λ
1.0
0.9
0.8
λ4471
0.15
Fe II, λ4472.9
Δλ
0.5 Å

FIGURE 6

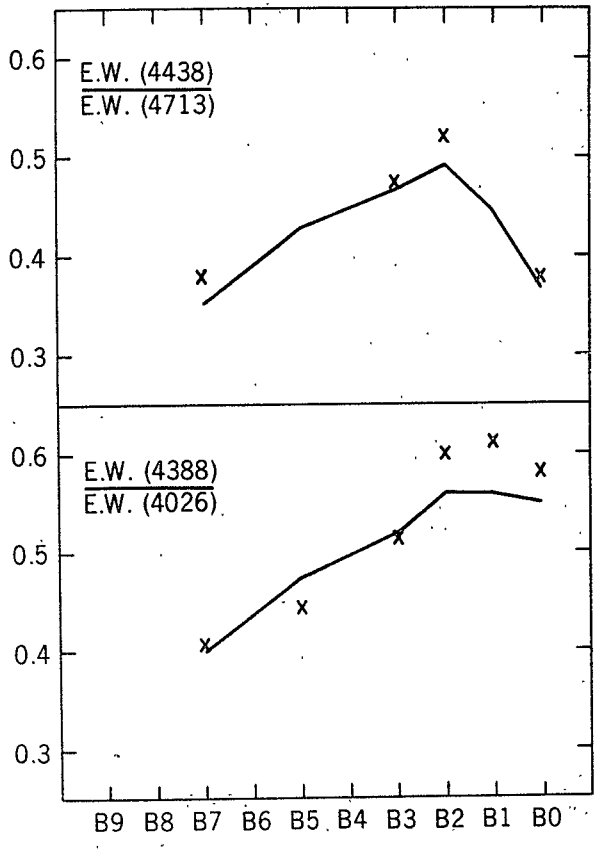
0.6
0.5
0.4
0.3
E.W. (4438)
E.W. (4713)
0.6
0.5
0.4
0.3
E.W. (4388)
E.W. (4026)
B9 B8 B7 B6 B5 B4 B3 B2 B1 B0

FIGURE 7